MR Imaging and MR Spectroscopy in Prostate Cancer

Winfried A. Willinek, Georges Decker, and Frank Träber

Contents

Abstract

Multiparametric MR Imaging with high resolution T2-weighted imaging (HR-T2WI), diffusion weighted imaging (DWI), dynamic contrast enhanced MRI (DCE-MRI), and MR spectroscopy (MRS) plays a crucial role in the assessment, localization, staging, biopsy planning, and therapy monitoring of prostate cancer (PCa) through delivering unmatched soft tissue contrast as well as functional information especially regarding cell density, vascularization, and metabolism. It also helps identifying tumors missed on PSA testing, DRE, and TRUS-guided biopsy. HR-T2WI provides a clear depiction of the prostate zonal anatomy and is indispensable for PCa detection, localization, and accurate tumor staging. DWI adds information about cellular density by quantifying Brownian motion of interstitial water molecules and thereby enabling the differentiation of benign from malignant tissue. DCE-MRI is another functional imaging technique which allows for characterizing pharmacokinetic features reflecting the prostatic vascularization through a series of high temporal resolution T1-weighted images following the administration of contrast medium. In-vivo proton MRS investigates the biochemical constituents of prostate tissue noninvasively. Metabolic alterations caused by cancerous infiltration can be identified as well as metabolic response in the course of radiotherapy. While in the healthy gland citrate provides the predominant signal in MR spectra, strong accumulation of choline compounds indicates PCa, and the choline/citrate ratio may serve as suitable biomarker for malignancy. MRS allows simultaneous acquisition of spatially localized spectra from a multitude of tissue volumes as small as 1 cm^3 or below, with complete prostate coverage.

W.A. Willinek (✉) · G. Decker · F. Träber
Department of Radiology, University of Bonn,
Sigmund-Freud-Str. 25, 53105 Bonn, Germany
e-mail: Winfried.Willinek@ukb.uni-bonn.de

H. Geinitz et al. (eds.), *Radiotherapy in Prostate Cancer*, Medical Radiology. Radiation Oncology,
DOI: 10.1007/174_2014_1034, © Springer-Verlag Berlin Heidelberg 2014
Published Online: 4 September 2014

1 The Role of Magnetic Resonance Imaging (MRI) in the Diagnosis and Therapy Monitoring of Prostate Cancer (PCa)

The diagnosis of prostate cancer (PCa) is mainly based on prostate-specific antigen (PSA) testing, digital rectal examination (DRE), and transrectal ultrasonography (TRUS) with optional TRUS-guided biopsy. All these tests have relevant limitations. PSA testing has a low specificity because some conditions such as infections or benign prostatic hyperplasia (BPH) can also induce PSA elevation (Romero Otero et al. 2014). Furthermore, some studies suggest that PSA testing does not provide an accurate surrogate measure of cancer cure or treatment efficacy up to the first 4–5 years after radiation therapy (Vicini et al. 2005). DRE only allows the posterior surface of the gland to be palpated and neither offers high specificity nor sensitivity nor is it suitable for therapy monitoring.

In case of a suspicious PSA or DRE result, initially a TRUS-guided sextant biopsy with acquisition of 12 cores minimum is recommended to be performed. Unfortunately, TRUS biopsy is prone to underestimating the prevalence and aggressiveness of the disease: about 35 % of PCas are missed by the first biopsy (Djavan et al. 2001) and the highest Gleason score is missed in about 46 % of cases (Noguchi et al. 2001). This often leads to insufficient diagnoses, inaccurate risk assessments, and ultimately a less-than-optimal therapy. Furthermore, patients with understaged PCa may undergo radical surgery without prognostic benefits.

About 15 % of PCa patients have normal PSA levels, and no tumor is palpable in DRE. Unfortunately, among these clinically silent tumors, about 15.6 % have a Gleason score ranging from 7 to 9 (Thompson et al. 2004). Recent studies reported a sensitivity and specificity by MRI of 84.2 and 66.6% respectively in the detection of clinically low-risk PCa with Gleason scores less than or equal to 6. In contrast, cancers with higher Gleason grades, i.e., clinically significant tumors, had a detection accuracy of about 90 % (Kim et al. 2014) and a negative predictive value of up to 95 % (Arumainayagam et al. 2013). Other research groups found diffusion-weighted imaging (DWI) at 3 Tesla (T) alone detecting significant PCa with a sensitivity and specificity ranging from 89 to 91 % and 77 to 81 %, respectively (Bains et al. 2014). These data enhance the important role of MRI in detecting those PCas that need more radical treatments.

Among imaging modalities, MRI is unmatched regarding the morphologic and functional evaluation of the prostate gland (Delongchamps et al. 2011). Computed tomography (CT) does not provide sufficient tissue contrast discrimination in the prostate. However, it is valuable in the assessment of pelvic lymph nodes and bone metastases, although MRI has been shown to be superior here too (Dotan 2008). A recent study with 922 patients who received prostate multiparametric MRI (mp-MRI) before radical prostatectomy reported a detection accuracy of 91 % for lymph node metastases with a negative prediction value of 94.5 % (Jeong et al. 2013).

MRI can not only help identifying tumors missed on PSA testing, DRE, and TRUS-guided biopsy but also increases biopsy yields if performed before biopsy through prior localization. This holds true especially in the anterior parts of the prostate gland, which are typically only difficult to reach by standard TRUS.

In the perspective of the above-mentioned limitations of PSA, DRE, and TRUS, MRI represents an attractive imaging modality with high spatial resolution and excellent soft tissue contrast. For many PCa patients, MRI is currently the only modality to delineate potentially malignant foci. In consequence, MRI of the prostate is increasingly used for detection and localization of PCa including consecutive radiation therapy and radiation boost planning.

Assessment of radiation therapy effectiveness, tumor recurrence, and therapy monitoring in PCa is still a challenge. Local recurrence of PCa is actually diagnosed by PSA kinetics. Unfortunately, patterns of PSA kinetics cannot conclusively differentiate between local therapy failure and distant metastasis (Roach et al. 2006). DRE is difficult to interpret during and after radiation therapy, due to associated effects such as induced fibrosis. MRI and especially DWI can reflect cellular changes in malignant tissue under radiotherapy (Song et al. 2010). With the recent technical advancements in MRI, preliminary studies showed that DWI plays an important role in detecting PCa recurrence after radiation therapy (Kim et al. 2009). Mp-MRI can also be useful in the planning of radiation therapy by providing important information for determination of the radiation boost and coverage (Chang et al. 2014).

With the increasing availability of 3T MR systems, MRI of PCa has dramatically improved. Most functional techniques in mp-MRI benefit when moving from 1.5 to 3 T (Lagemaat and Scheenen 2014). The intrinsic signal-to-noise gain at 3 T allows for replacement of the endorectal coil by phased-array coils which enhances patient comfort and compliance. In the future, combined MR-PET may add further molecular targets to the multiparametric information that is provided already today. However, published data are still limited, and further studies are necessary to establish the clinical role of hybrid imaging in PCa.

Over all, according to the authors' opinion, state-of-the-art MR imaging is indispensable in the modern, interdisciplinary work-up of PCa prioritizing T2-weighted and diffusion-weighted sequences.

2 Multiparametric MRI (mp-MRI)

The first prostate MRI was performed in the mid-1980s (Steyn and Smith 1984). Ever since then, prostate MRI developed from a promising tool to a mature imaging modality, gathering not only morphological but also functional information. State-of-the-art mp-MRI preferably performed at 3 T nowadays includes T2- and T1-weighted imaging yielding morphological information as well as DWI, dynamic-contrast-enhanced perfusion (DCE-MRI), and MR spectroscopy (MRS) providing primarily functional information (Table 1).

Bowel motion artefacts can be reduced by administering an antiperistaltic agent such as butylscopolaminbromid. Patients should be instructed about the importance of not moving during image acquisition. An endorectal coil (ERC) is not an absolute requirement at either 1.5 T or 3 T anymore, but strongly recommended for imaging at 1.5 T (Beyersdorff et al. 2003). 3 T MRI scanners and the associated higher signal-to-noise ratio (SNR) provide excellent image quality without ERCs, which in turn translates generally in better patient acceptance. Phased-array coils with multiple receiving channels are currently used in standard clinical practice.

2.1 T2-Weighted Imaging

T2-weighted imaging (T2WI) can provide high spatial resolution and clear depiction of the zonal anatomy of the prostate and therefore is indispensable for PCa detection, localization, and accurate tumor staging. Anatomically, the prostate gland has four distinct glandular regions, the peripheral zone, central zone, transition zone, and the anterior fibromuscular zone.

A healthy peripheral zone has homogeneous high signal intensity (SI) on T2-weighted images, as it consists mostly of glandular structures. The central zone has variable amounts of inhomogeneous intermediate SI. Several studies in the late 1980s established that PCa in the peripheral zone is characterized by low T2 SI. This is due to unrestricted growing of cancer cells that do not preserve the glandular structure of the peripheral zone (Bezzi et al. 1988) (Fig. 1).

In the central and transition zone, an irregular low-SI area without capsule resembling an “erased charcoal” or a SI-disrespecting normal glandular structure, the capsule or the urethra is considered malignant. High-grade cancers usually have a lower SI than low-grade cancers (Wang et al. 2008).

Interpretation of T2WI includes the evaluation of all adjacent structures in the male pelvis, especially capsule, seminal vesicles, and posterior bladder wall for extraprostatic tumor invasion as well as for lymph nodes and bone structures regarding lymphogenic or haematogenic tumor spread.

Table 1 Landmark studies correlating imaging modalities with histopathological results

mp-MRI	Histopathological correlation	References
HR T2	Glandular morphology	Bezzi et al. (1988)
DWI	Gleason score	Turkbey et al. (2011)
DCE-MRI	Neoangiogenesis	Engelbrecht et al. (2003)
MRS	Cell metabolism	Costello and Franklin (1997)

Sensitivity and specificity for T2WI differ among studies, Turkbey et al. found a sensitivity of 42 % and specificity of 83 % across all prostatic regions (Turkbey et al. 2010).

One drawback of T2WI alone is the limited specificity of low-SI areas. Benign abnormalities such as chronic prostatitis, atrophy, scars, postirradiation or antihormonal treatment effects, hyperplasia, and postbiopsy hemorrhage may mimic a low-SI-resembling tumor tissue (Kirkham et al. 2006).

2.2 Diffusion-Weighted Imaging (DWI) and the Apparent Diffusion Coefficient (ADC)

DWI adds important information about cellular density on a tissue level to the morphological information from high-resolution T2WI.

DWI as noninvasive, functional MR technique quantifies the Brownian motion of water molecules within tissue. Thereby, it enables not only qualitative but also quantitative tumor assessment. Reduced water diffusion in PCa has been attributed to increased cellularity through uncontrolled tumor growth with a consecutive reduction of the extracellular space. Therefore, DWI primarily provides an important quantitative biophysical parameter that can be used to differentiate benign from malignant prostatic tissue that shows the typical pattern of high SI on images with high b-values and low SI on the ADC map (Hosseinzadeh and Schwarz 2004) (Fig. 2a, b).

DWI in combination with T2WI is not only clinically relevant for improved tumor detection and characterization, but also increasingly used for therapy monitoring before, during, and after treatment (Chenevert et al. 2002). There is evidence that DWI allows to reflect cellular changes in malignant tissue, especially under radiation (Song et al. 2010).

DWI acquisition parameters should be optimized according to the respective MR imaging system as well as to the magnetic field strength that is implemented. The acquisition of at least two different b-values, which specify the sensitivity

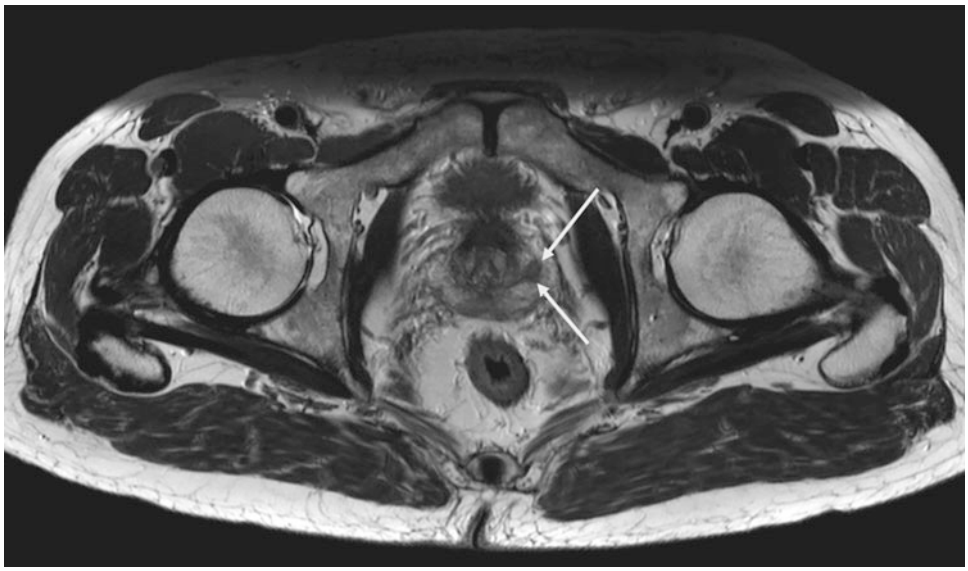

Fig. 1 Axial high resolution T2-weighted TSE showing a PCa lesion in the left peripheral zone (*white arrows*)

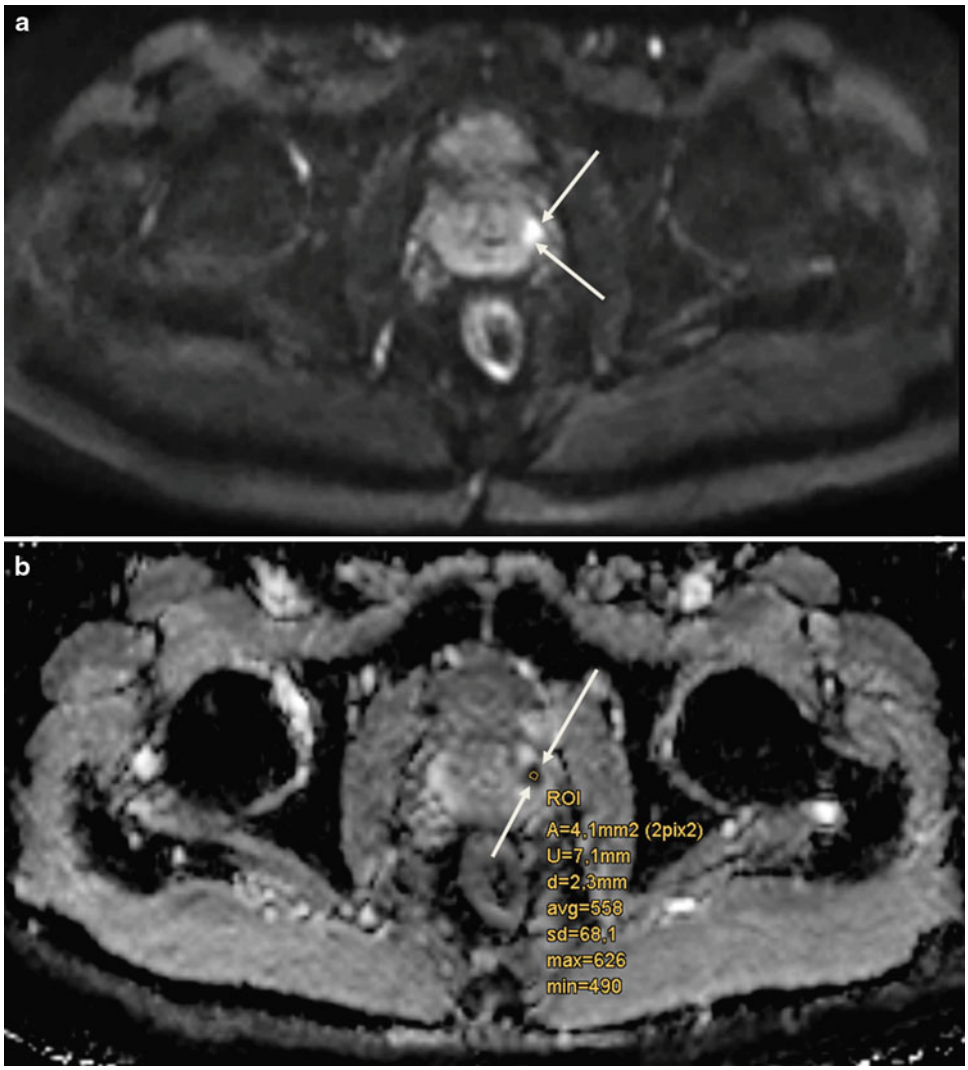

Fig. 2 **a** Axial DWI (b = 800 mm^2/s) highlighting a PCa in the left peripheral zone (*white arrows*) and **b** corresponding axial ADC map

of diffusion weighting, is a prerequisite for the calculation of ADC maps for accurate quantitative analysis. Selection of the appropriate b-values for DWI is crucial because higher b-values increase the sensitivity to detect changes in diffusion, but at the same time impair the signal-to-noise ratio. Benefits of DWI are the relatively short acquisition time and high contrast resolution between tumors and normal tissue that is comparable to positron emission tomography (PET; "PET-like imaging"). A shortcoming of DWI is the vulnerability to susceptibility-induced distortion artefacts due to air/tissue interfaces, for example, at the boundary of the rectal wall.

DWI and the calculated apparent diffusion coefficient (ADC) in particular have initially been used to assess tumor aggressiveness, especially in brain cancers (Sugahara et al. 1999). In the meantime, several groups found out that ADCs obtained from DWI were significantly lower in PCas with higher Gleason scores (Turkbey et al. 2011). This allows for noninvasive assessment of the aggressiveness of PCas that are visible on MR images, which is an important predictor for patient outcome, prognosis, and can also be useful in the planning of radiation therapy.

2.3 Dynamic-Contrast-Enhanced MRI (DCE-MRI, Perfusion Imaging)

DCE-MRI is a functional imaging modality following the intravenous (i.v.) administration of gadolinium-based contrast medium allowing the characterization of pharmacokinetic features reflecting the prostatic vascularization through a series of high temporal resolution axial T1-weighted sequences.

Vascularization and angiogenesis in PCa are mostly induced through the secretion of vascular growth factors in reaction to the presence of local hypoxia or lack of nutrients due to uncontrolled fast growth of malignant cells (Bonekamp and Macura 2008). The resulting changes on a vascular level can be assessed dynamically by DCE-MRI. As the prostate gland is highly vascularized, a simple substraction of images before and after gadolinium administration i.v. is insufficient to properly delineate PCa, and a dynamic imaging series with adequate temporal resolution is required instead to accurately determine the time course of contrast media inflow and washout.

Tumor vessels are generally more permeable and disorganized than normal vessels. Because of the abundance of tumor vessels in PCa and the corresponding vessel walls' vulnerability and permeability, fast contrast arrival and rapid washout are typically observed (Fig. 3a, b). It has been demonstrated that the presence of washout is highly indicative for PCa (Alonzi et al. 2007), even in the absence of low SI in T2WI.

2.4 MR Spectroscopy of Prostate Cancer

2.4.1 ^{1}H-MR Spectrum and Metabolite Signals

While the morphologic and functional properties of normal or neoplastic tissue in the prostate gland can be delineated by MR imaging methods, in vivo proton MR spectroscopy (^{1}H-MRS) and spectroscopic imaging (^{1}H-MRSI) investigate its chemical composition noninvasively and thus yield further insight into prostate metabolism and the metabolic alterations caused by cancerous infiltration. Also, metabolic changes in the course of radiotherapy can be monitored, and the response of PCa to treatment may be assessed by MRS and MRSI. Of the metabolites present in the prostate gland, citrate (Cit), creatine/phosphocreatine (Cr), choline-containing compounds (Cho), and polyamines (PA) have sufficiently high tissue concentrations (above 1 mmol/kg) to be detected by MRS at the magnetic field strengths used for in vivo examinations. Cit is produced by oxidative phosphorylation within the citrate cycle and is extensively stored in healthy prostate tissue mainly in bound form as zinc citrate (Costello et al. 2005). It has a ^{1}H-MRS resonance at 2.65 ppm (chemical shift relative to tetramethylsilane as reference) arising from the non-equivalent methylene protons (CH_2) which are strongly coupled to form two almost overlapping spin doublets. This leads to a characteristic 4-peak spectral pattern at 3 T with two equally high central peaks spaced by 8 Hz and two smaller "outer" satellites each at 16 Hz distance (corresponding to the J coupling constant of Cit) from the central peaks. However, full resolution of all 4 peaks is achieved in vivo only with excellent magnetic field homogeneity, while in many prostate MRS acquisitions at 3 T, the two central constituents appear as a single broadened peak, which is a general issue at the lower field of 1.5 T. Also, the three methyl resonances of Cho, PA, and Cr covering the spectral range of 3.21–3.03 ppm are often not completely resolved, especially at 1.5 T, and therefore, usually the summed intensity (tChoCr) of all peaks in this frequency range is compared to the total area under the citrate components, yielding a metabolite ratio, e.g. called tChoCr/Cit.

Although being itself a complex overlay of several constituents such as glycerol phosphorylcholine (GPC), phosphorylcholine (PC), acetylcholine (ACho), and free choline, the intensity of the Cho peak centered at 3.21 ppm in the proton spectrum of prostate tissue may serve as a biomarker for the detection of malignant disease, just in analogy to the PSA value, with strongly increased Cho level or ratio Cho/Cit being suspicious for PCa (Cornel et al. 1993). As especially the phospholipids GPC and PC are key components released in cell membrane turnover, extensive cell proliferation as it is found in malignant tumors is often accompanied by a characteristic elevation of the choline peak in the ^{1}H-MR spectrum. Simultaneously, the accumulation of

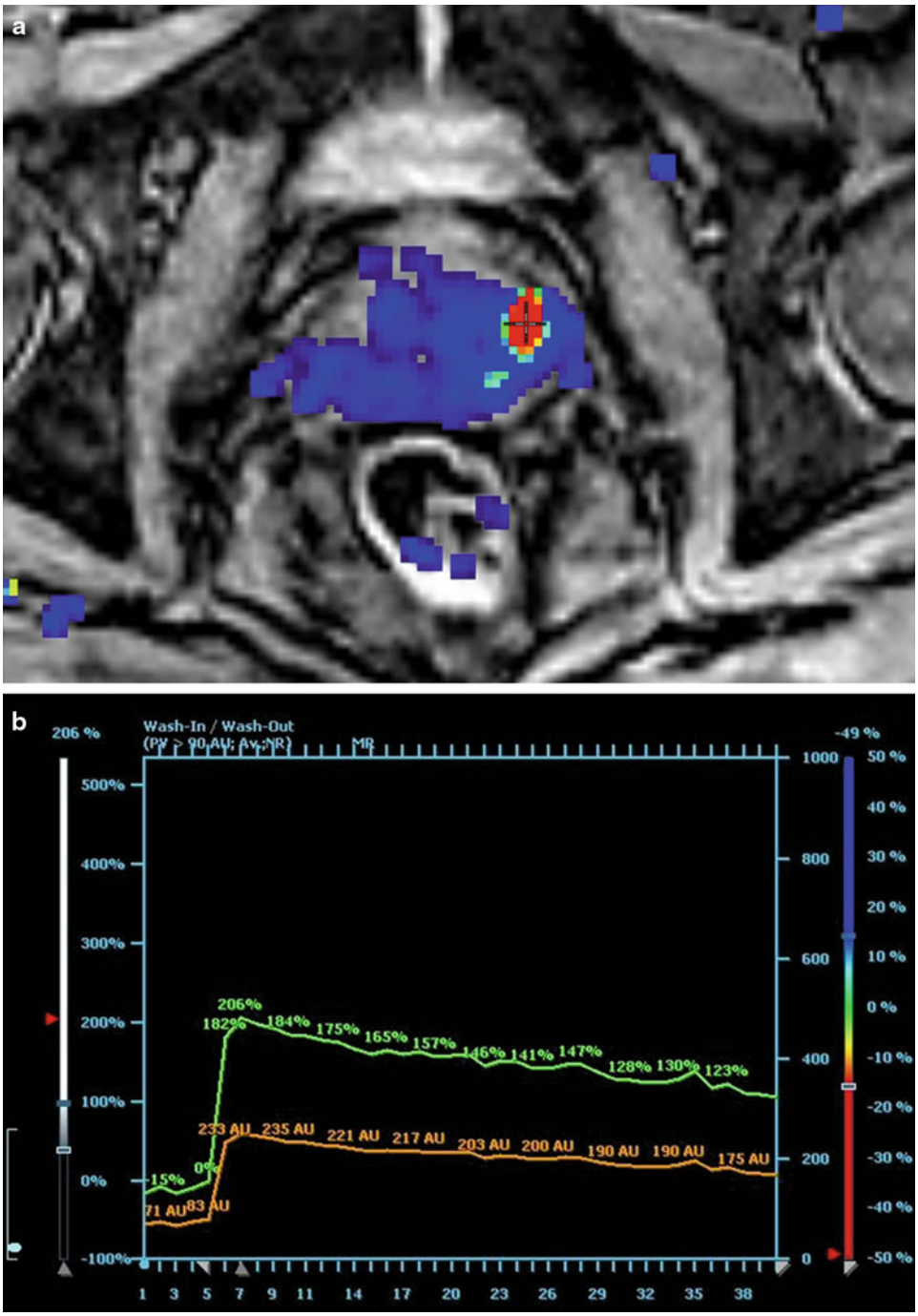

Fig. 3 **a** Axial high temporal resolution DCE-MRI with a PCa lesion in the left peripheral zone (*red spot*). **b** Corresponding enhancement curve with relative (*green curve*) and absolute (*orange curve*) depiction of contrast enhancement arrival and consecutive washout

citrate is inhibited in cancerous prostate tissue, and the MRS intensity of the citrate peaks decreases (Costello and Franklin 1997). Therefore, both effects add up to increase the metabolite ratio Cho/Cit. In contrast, the summed area tChoCr under the Cho, PA, and Cr spectral peaks and its ratio to Cit are less sensitive to indicate PCa, because an elevation in choline levels is at least partly counterbalanced by a reduction of Cr and PA in affected tissue. Nevertheless, in cases or at field strengths with insufficient spectral separation of Cho from the adjacent PA and Cr peaks, the tChoCr/Cit ratio may still serve as a suitable marker to discriminate between benign tissue and PCa, with values <0.8 being considered as normal and tChoCr/Cit >1 as highly suspicious for malignant disease. Correspondingly, a Cho/Cit ratio below 0.5 may indicate benign hyperplasia, while Cho/Cit ratio >0.6 suspects PCa, with borderline assignment for values in between (Crehange et al. 2011). However, such thresholds have to be regarded with care as they may vary depending on the used field strength, the scan parameters (mainly TR and TE) of the MRS acquisition sequence, and the achieved spectral peak

resolution. Moreover, the metabolite ratios differ between the prostate zones (with normal Cho/Cit being lower in the peripheral zone), and the cutoff values for discrimination between benign tissue and tumor have to be adjusted to the respective location within the gland.

While ^{1}H-MRS has been shown to be rather specific in the detection of PCa (89–91 % specificity), its sensitivity (75–77 %) is still inferior to other modalities (Manenti et al. 2006). One reason for missing a PCa lesion might be a too small or lacking increase of choline in tumors with only moderate cell proliferation, which is possibly associated with a lower Gleason score. Such a correlation between the Gleason score and the Cho levels in MRS has been found in some, but not in all studies (Zakian et al. 2005; Scheenen et al. 2007; Kobus et al. 2011). Also, PCa with focal size less than 1 cm is prone to be missed by MRS due to its limited spatial resolution, resulting in partial volume averaging with healthy tissue and thus yielding metabolite ratios below the chosen malignancy threshold. On the other hand, false-positive findings may be derived from high Cho signal also occurring in prostatitis, or if an intense narrow spectral peak is observed in MR spectra from the posterior parts in the basal region of the prostate, at the choline frequency of 3.2 ppm. This signal can be assigned to GPC contained in the seminal vesicles, and attention has to be paid not to mistake this "normal" GPC peak from seminal fluid with a pathological elevation of choline levels suspecting prostate cancer in that region.

2.4.2 ^{1}H-MRS Acquisition and Spatial Localization

The achievable spatial resolution for in vivo prostate MRS is one of the major drawbacks of this technique as the size of a tissue volume from which a proton MR spectrum is obtained by far exceeds the spatial dimensions of all other MR imaging methods and of most other imaging modalities. This is a consequence of the more than 10,000-fold lower tissue concentrations of the ^{1}H metabolites of interest (Cho, Cr, Cit) compared to the water protons used in MR imaging. Moreover, the intense spectral peak of water at 4.7 ppm has to be suppressed by suitable prepulses during MRS acquisition (and additionally by filtering algorithms in MRS postprocessing) to allow reliable quantification of the very small metabolite peaks, even when their chemical shift relative to water is quite large. Also, MRS signals from different molecular groups in lipids may overlay and distort the metabolite peaks, particularly of citrate, if the selected MRS volume partially includes fatty tissue. In localized single-volume (SV) ^{1}H-MRS, the metabolite signals are collected from within a brick-shaped tissue volume interactively placed on localizer MR images, which is selected by combining the excitation and refocusing RF pulses with magnetic field gradients for spatial encoding. This volume selection can be performed either with the point-resolved spectroscopy (PRESS) (Bottomley 1987) or the stimulated echo acquisition mode (STEAM) (Frahm et al. 1989) technique. Although the SNR of the metabolite peaks in the acquired MR spectra can strongly be improved by repeating the excitation of the volume of interest (VOI) and accumulating the MRS data ("signal averaging"), this may lead to unacceptably long measurement times if VOI sizes smaller than 2–3 cm^3 are desired, even at higher magnetic fields with their inherently better SNR. Therefore, in MRS of the prostate, SV techniques are not suited for accurate localization of a tumor within the tissue as the required VOI size would extend over a much too large part of the prostate gland. SV-MRS of prostate cancer might thus only be of interest if the tumor site is already known and the time course of progression or response to therapy is to be investigated in consecutive examinations.

2.4.3 MR Spectroscopic Imaging (MRSI)

By application of the MRSI technique (often also called chemical shift imaging (CSI)), a 2D or 3D grid consisting of a multitude of smaller voxels can be used to collect MR spectra from each of these voxels. To achieve this, similar to the principles of MR imaging, slice selection is performed by gradient switching during RF excitation, and additional phase encoding is applied for in-plane localization. In contrast to the MR imaging of water protons, however, it is not possible to use frequency encoding to acquire a complete row of the image following a single excitation, because the different frequency components of the detected MRS signal are already linked to the spectral information on the metabolites of interest. Therefore, phase encoding for two spatial directions (or even three in 3D-MRSI) has to be used, and as a consequence, m × n spin excitations spaced by the repetition time TR have to be performed to acquire the desired matrix of m × n MR spectra from all 2D grid voxels. Fortunately, the SNR in these spectra is not determined by the spin signal only from the corresponding small voxel, but from the total MRSI grid which above all is sampled m × n times and accumulated. In this way, in-plane voxel sizes around 1 cm^2 or below can be utilized with sufficient metabolite SNR in 2D-MRSI of the prostate, with typically 10 × 10–16 × 16 voxels over a grid extension of 8–12 cm. Because a field of view (FOV) of this size is completely surrounded by body tissue, back-folding of spin signal from outer structures would happen, like in MR imaging with such a small FOV, if only the 2D phase encoding was used for in-plane volume selection. Therefore, additional PRESS or STEAM localization of a VOI smaller than the margins of the phase-encoded FOV but completely covering the prostate gland has to be applied to avoid artificial signal contribution in the spectra of the MRSI voxels, especially from lipids. Suppression of such "outer volume" signals can also be achieved by multiple regional presaturation bars closely

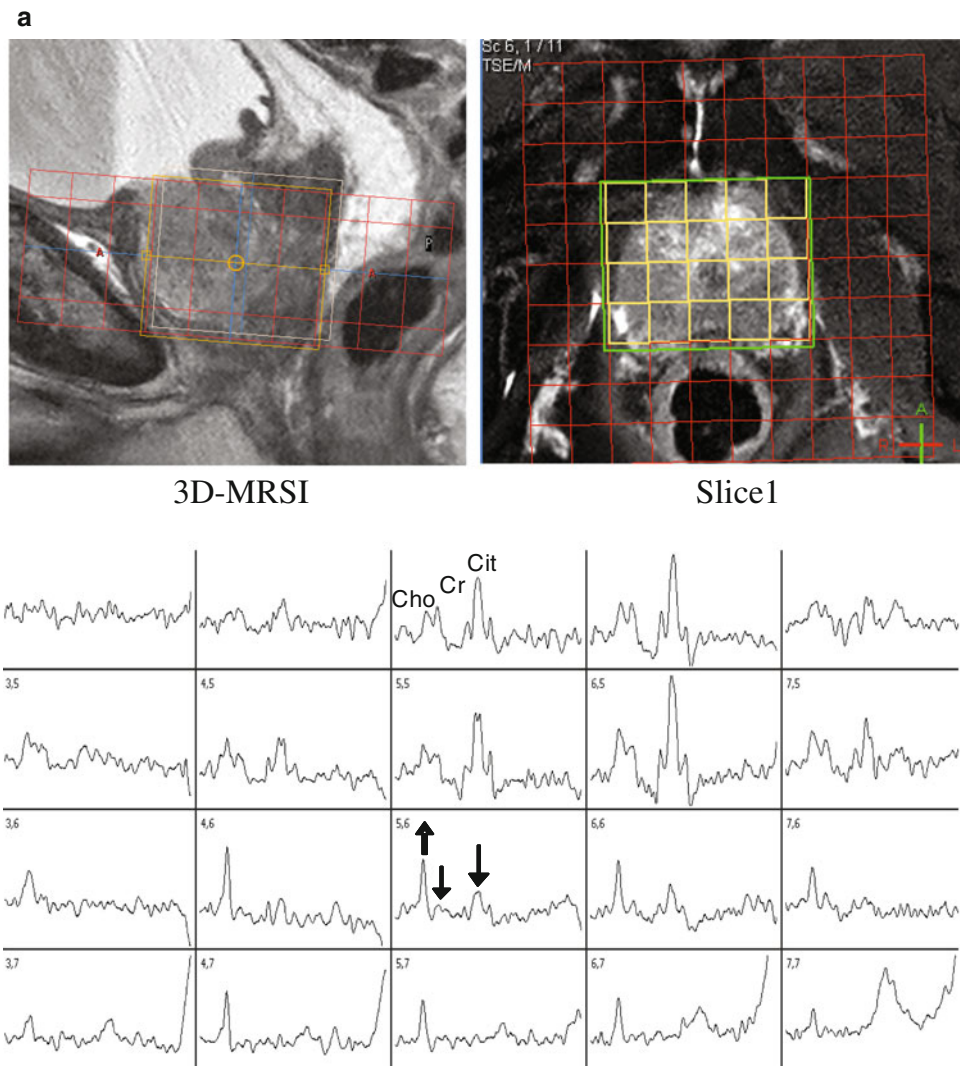

Fig. 4 3D-MRSI (TR/TE 1200/135 ms, acquisition matrix 10 × 10 × 3) of the prostate with external surface coil at 3T in a 74-year-old patient before radiotherapy. Overlay of MRSI grid (*red*) of isotropic 1-cm voxels and PRESS selection volume (*green frame*) on sagittal and transversal T2W MR images, and 2D array of selected MR spectra arranged corresponding to the yellow-framed voxels. **a** Spectra from MRSI slice #1 (at the prostate apex) show normal metabolite levels in the anterior part of the gland and demonstrate prostate cancer focused right posterior, indicated by strongly enlarged choline in association with barely detectable citrate (see up/*down arrows*). **b** Acquired (*red*) and fitted (*blue on green baseline*) spectra from 4 voxels in central MRSI slice (#2) show steep transition from unaffected area (*upper row*) to clearly malignant tissue (*lower row*) in directly adjacent voxels. Vertical scaling of spectra in (**b**) different from (**a**)

adapted to the individual prostate shape. In most cases, the cranio-caudal size of the prostate is too large to be entirely included in a 2D-MRSI acquisition with a slice thickness of 1–2 cm, and a 3D phase encoding scheme with at least three axial slices has to be used then. Fig. 4 shows an example for the image-guided planning of such a 3D-MRSI acquisition (TR/TE 1200/135 ms) with display of the 10 × 10 × 3 voxel grid (red), the PRESS-localized VOI (green frame), and a selection of spectra (yellow-framed voxels) from the peripheral and from the central zone of the prostate within the VOI. In this examination performed before radiotherapy, a high Cho peak and low Cit level indicating extensive tumorous infiltration are present in the spectra from the posterior region of the prostate, with accentuation in the right glandular lobe and apical. Just as the other techniques of multiparametric MR imaging, also MRS and MRSI of the prostate profit from the signal gain achievable by the use of an endorectal RF coil for signal detection, and its application allows to further decrease the minimum voxel size. While at magnetic fields of 2 T or less, the application of ERCs for prostate MRSI is mandatory, at 3 T the inherently higher MR signal and the stronger sensitivity to susceptibility artifacts caused by the endorectal placement might balance out the advantages of such coils. Therefore, also considering the signal increase gained by recent progress in MR detection sensitivity by digital RF chains and coil development, the sole use of external surface coils will at 3 T supply sufficient SNR and spatial resolution for MRSI, combined with more patient comfort.

Corresponding to the cutoff values for the metabolite ratios tChoCr/Cit and Cho/Cit cited before, but on a less stringent scale and thus more considering the dependency of such limits on the location within the prostate gland and on the MRS scan parameters, the new PI-RADS diagnostic grading of prostate lesions has been extended also to assessment by MRS (Barentsz et al. 2012). In the qualitative scoring of MRSI, only the peak heights for Cho and Cit are compared, from PI-RADS 5 corresponding to “Cho>>Cit,

Fig. 4 continued

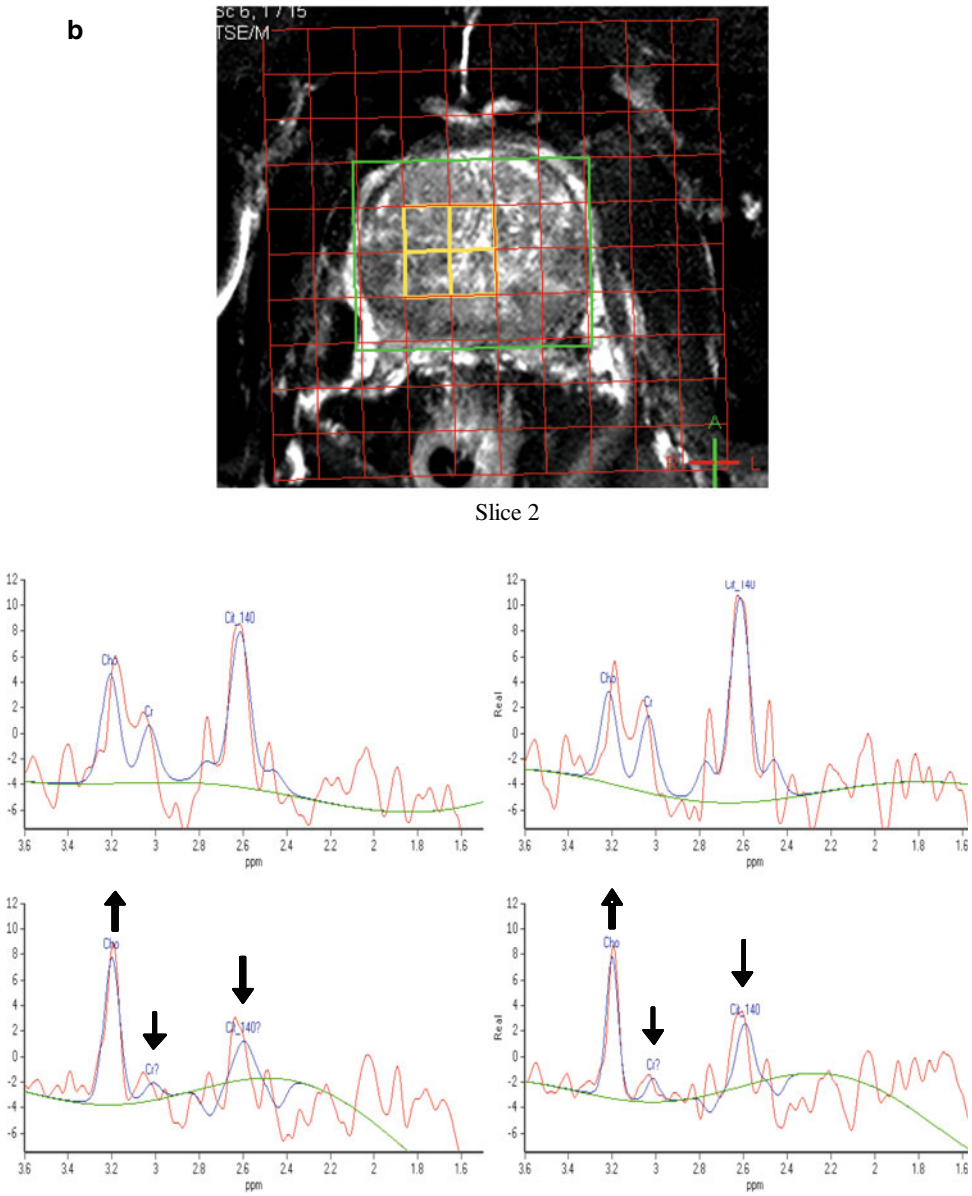

cancer is highly likely to be present" down to PI-RADS 1, assigned when "Cho<<Cit, disease is highly unlikely to be present."

2.4.4 MRSI of the Prostate in Radiotherapy Planning and Follow-Up

While the criteria described above can successfully be applied in the differential diagnosis between malignant disease and benign hyperplasia by MRS and in the localization of tissue with cancerous infiltration to define the target area in radiotherapy planning, a severe problem is encountered when response to therapy or residual/recurrent tumor has to be assessed by MRS in follow-up examinations after or during the course of radiation therapy: The citrate levels in irradiated prostate tissue are strongly decreased due to the metabolic damage induced by the radiation ["metabolic atrophy" (Pickett et al. 2004)], and recovery will not be achieved even years after the end of therapy. Therefore, all metabolite ratios with Cit as denominator will distinctly be elevated almost immediately after the first few radiotherapy fractions even when the tumor responds well and degrades in the course of irradiation. Figure 5 displays the typical alterations of metabolite levels in the course of radiotherapy in a case with prostate cancer located in the left central and peripheral zone, with very low amplitudes of all metabolite signals at therapy cessation demonstrating metabolic atrophy. A similar decline of the citrate levels (and corresponding increase of Cho/Cit and tChoCr/Cit) can also be seen in MRS already before radiotherapy in patients with adjuvant antihormonal therapy (Mueller-Lisse et al. 2007).

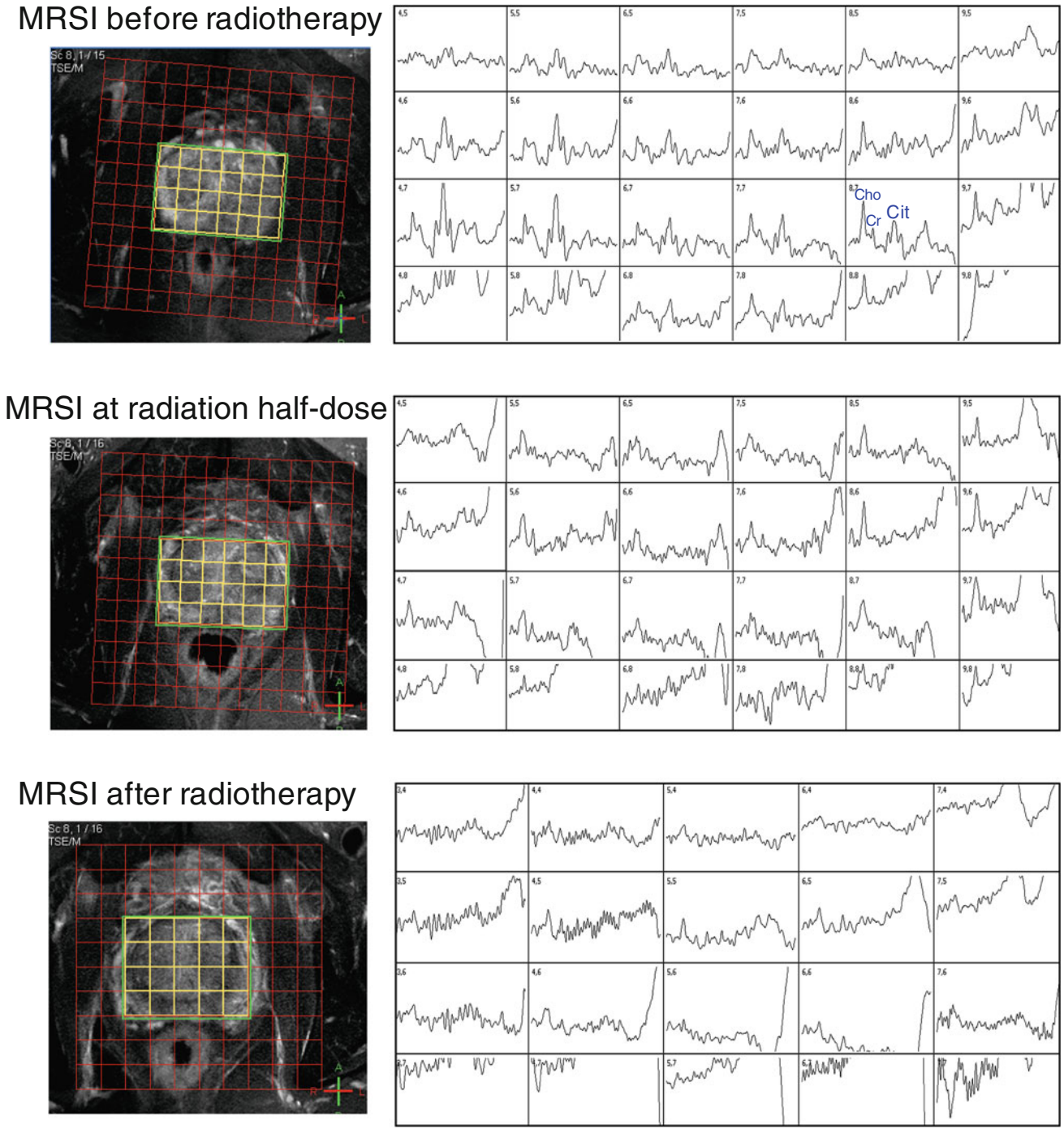

Fig. 5 MRSI at 3 T in the course of radiation therapy of prostate cancer in a 77-year-old patient. Display of MRSI grid and selected voxels within PRESS volume on fat-suppressed TSE and corresponding array of MR spectra acquired before the first therapy session (*upper row*), after reaching half of the total radiation dose (*middle row*) and shortly after the last therapy fraction (*lower row*). Initially, high Cho peak and reduced Cr and Cit signals in almost all spectra from the left glandular lobe indicate the cancerous infiltration. After reaching half of the total dose, citrate is no more detectable anywhere in prostate tissue, but Cho/Cr still remains elevated at the tumor location. In the examination after therapy, only very few MR spectra show metabolite signals above noise level, and this "metabolic atrophy" may be associated with a successful response to radiotherapy

As the ratios Cho/Cr or Cho/(Cr+PA) will not be affected that much by radiation-induced metabolic alterations, strongly increased values or even the mere identification of a distinct Cho peak in certain MRSI voxels may then serve as remaining indicators for tumor residue or recurrence (Westphalen et al. 2010). However, clear cutoff values for

these ratios cannot be defined easily, and due to general signal reduction of all metabolites in the course of radiotherapy, an artificial elevation in low-SNR spectra may also be observed. In addition, a final decrease in initially high values for Cho/Cr or Cho/(Cr+PA), indicating metabolic atrophy (and thus a successful response to radiotherapy), may be delayed even for months after therapy cessation. Therefore, in our experience, MR spectroscopy in the radiotherapy of prostate cancer should comprise an MRSI acquisition straight before the beginning of therapy (including antihormonal treatment) to assess tumor location and extension within the gland for a possible definition of target tissue for radiation boosts, and follow-up MRSI not before several months after therapy end to check for focal remaining or newly rising high choline levels. Nevertheless, the relevance of posttherapy choline and citrate levels in irradiated prostate tissue as prognostic factors for relapse-free survival or for tumor recurrence still remains a controversial issue and has to be investigated in further studies.

3 Summary

Multiparametric MR imaging and MR spectroscopy play a pivotal role in the assessment of prostate cancer. Current imaging should include morphology (T2-weighting), diffusion, perfusion, and spectroscopy, preferably at higher field strengths such as 3 T. State-of-the-art imaging allows for tumor detection, local tumor staging, and therapy monitoring. Future studies will provide even more evidence for the value of MR imaging and MR spectroscopy, especially in the context of therapy decision making.

References

Alonzi R, Padhani AR, Allen C (2007) Dynamic contrast enhanced MRI in prostate cancer. Eur J Radiol 63:335–350. doi:10.1016/j.ejrad.2007.06.028

Arumainayagam N, Ahmed HU, Moore CM et al (2013) Multiparametric MR imaging for detection of clinically significant prostate cancer: a validation cohort study with transperineal template prostate mapping as the reference standard. Radiology 268:761–769. doi:10.1148/radiol.13120641

Bains LJ, Studer UE, Froehlich JM et al (2014) Diffusion-weighted magnetic resonance imaging detects significant prostate cancer with a high probability: results of a prospective study with final pathology of prostates with and without cancer as the reference standard. J Urol. doi:10.1016/j.juro.2014.03.039

Barentsz JO, Richenberg J, Clements R et al (2012) ESUR prostate MR guidelines 2012. Eur Radiol 22:746–757. doi:10.1007/s00330-011-2377-y

Beyersdorff D, Darsow U, Stephan C et al (2003) MRI of prostate cancer using three different coil systems: image quality, tumor detection, and staging. RöFo Fortschritte Auf Dem Geb Röntgenstrahlen Nukl 175:799–805. doi:10.1055/s-2003-39929

Bezzi M, Kressel HY, Allen KS et al (1988) Prostatic carcinoma: staging with MR imaging at 1.5 T. Radiology 169:339–346. doi:10.1148/radiology.169.2.3174982

Bonekamp D, Macura KJ (2008) Dynamic contrast-enhanced magnetic resonance imaging in the evaluation of the prostate. Top Magn Reson Imaging TMRI 19:273–284. doi:10.1097/RMR.0b013e3181aacdc2

Bottomley PA (1987) Spatial localization in NMR spectroscopy in vivo. Ann N Y Acad Sci 508:333–348

Chang JH, Lim Joon D, Nguyen BT et al (2014) MRI scans significantly change target coverage decisions in radical radiotherapy for prostate cancer. J Med Imaging Radiat Oncol 58:237–243. doi:10.1111/1754-9485.12107

Chenevert TL, Meyer CR, Moffat BA et al (2002) Diffusion MRI: a new strategy for assessment of cancer therapeutic efficacy. Mol Imaging 1:336–343

Cornel EB, Smits GA, Oosterhof GO et al (1993) Characterization of human prostate cancer, benign prostatic hyperplasia and normal prostate by in vitro 1H and 31P magnetic resonance spectroscopy. J Urol 150:2019–2024

Costello LC, Franklin RB (1997) Citrate metabolism of normal and malignant prostate epithelial cells. Urology 50:3–12. doi:10.1016/S0090-4295(97)00124-6

Costello LC, Franklin RB, Feng P (2005) Mitochondrial function, zinc, and intermediary metabolism relationships in normal prostate and prostate cancer. Mitochondrion 5:143–153. doi:10.1016/j.mito.2005.02.001

Crehange G, Maingon P, Gauthier M et al (2011) Early choline levels from 3-tesla MR spectroscopy after exclusive radiation therapy in patients with clinically localized prostate cancer are predictive of plasmatic levels of PSA at 1 year. Int J Radiat Oncol Biol Phys 81:e407–413. doi:10.1016/j.ijrobp.2011.03.008

Delongchamps NB, Rouanne M, Flam T et al (2011) Multiparametric magnetic resonance imaging for the detection and localization of prostate cancer: combination of T2-weighted, dynamic contrast-enhanced and diffusion-weighted imaging. BJU Int 107:1411–1418. doi:10.1111/j.1464-410X.2010.09808.x

Djavan B, Ravery V, Zlotta A et al (2001) Prospective evaluation of prostate cancer detected on biopsies 1, 2, 3 and 4: when should we stop? J Urol 166:1679–1683

Dotan ZA (2008) Bone imaging in prostate cancer. Nat Clin Pract Urol 5:434–444. doi:10.1038/ncpuro1190

Engelbrecht MR, Huisman HJ, Laheij RJF et al (2003) Discrimination of prostate cancer from normal peripheral zone and central gland tissue by using dynamic contrast-enhanced MR imaging. Radiology 229:248–254. doi:10.1148/radiol.2291020200

Frahm J, Bruhn H, Gyngell ML et al (1989) Localized high-resolution proton NMR spectroscopy using stimulated echoes: initial applications to human brain in vivo. Magn Reson Med Off J Soc Magn Reson Med Soc Magn Reson Med 9:79–93

Hosseinzadeh K, Schwarz SD (2004) Endorectal diffusion-weighted imaging in prostate cancer to differentiate malignant and benign peripheral zone tissue. J Magn Reson Imaging JMRI 20:654–661. doi:10.1002/jmri.20159

Jeong IG, Lim JH, You D et al (2013) Incremental value of magnetic resonance imaging for clinically high risk prostate cancer in 922 radical prostatectomies. J Urol 190:2054–2060. doi:10.1016/j.juro.2013.06.035

Kim CK, Park BK, Lee HM (2009) Prediction of locally recurrent prostate cancer after radiation therapy: Incremental value of 3T diffusion-weighted MRI. J Magn Reson Imaging 29:391–397. doi:10.1002/jmri.21645

Kim JY, Kim SH, Kim YH et al (2014) Low-risk prostate cancer: the accuracy of multiparametric mr imaging for detection. Radiology 130801. doi: 10.1148/radiol.13130801

Kirkham APS, Emberton M, Allen C (2006) How good is MRI at detecting and characterising cancer within the prostate? Eur Urol 50:1163–1174; discussion 1175. doi: 10.1016/j.eururo.2006.06.025

Kobus T, Hambrock T, Hulsbergen-van de Kaa CA et al (2011) In vivo assessment of prostate cancer aggressiveness using magnetic resonance spectroscopic imaging at 3 T with an Endorectal coil. Eur Urol 60:1074–1080. doi:10.1016/j.eururo.2011.03.002

Lagemaat MW, Scheenen TWJ (2014) Role of high-field MR in studies of localized prostate cancer. NMR Biomed 27:67–79. doi:10.1002/nbm.2967

Manenti G, Squillaci E, Carlani M et al (2006) Magnetic resonance imaging of the prostate with spectroscopic imaging using a surface coil initial clinical experience. Radiol Med (Torino) 111:22–32

Mueller-Lisse UG, Swanson MG, Vigneron DB, Kurhanewicz J (2007) Magnetic resonance spectroscopy in patients with locally confined prostate cancer: association of prostatic citrate and metabolic atrophy with time on hormone deprivation therapy, PSA level, and biopsy Gleason score. Eur Radiol 17:371–378. doi:10.1007/s00330-006-0321-3

Noguchi M, Stamey TA, McNeal JE, Yemoto CM (2001) Relationship between systematic biopsies and histological features of 222 radical prostatectomy specimens: lack of prediction of tumor significance for men with nonpalpable prostate cancer. J Urol 166:104–109; discussion 109–110

Pickett B, Ten Haken RK, Kurhanewicz J et al (2004) Time to metabolic atrophy after permanent prostate seed implantation based on magnetic resonance spectroscopic imaging. Int J Radiat Oncol Biol Phys 59:665–673. doi:10.1016/j.ijrobp.2003.11.024

Roach M 3rd, Hanks G, Thames H Jr et al (2006) Defining biochemical failure following radiotherapy with or without hormonal therapy in men with clinically localized prostate cancer: recommendations of the RTOG-ASTRO phoenix consensus conference. Int J Radiat Oncol Biol Phys 65:965–974. doi:10.1016/j.ijrobp.2006.04.029

Romero Otero J, Garcia Gomez B, Campos Juanatey F, Touijer KA (2014) Prostate cancer biomarkers: an update. Urol Oncol. doi:10.1016/j.urolonc.2013.09.017

Scheenen TWJ, Heijmink SWTPJ, Roell SA et al (2007) Three-dimensional proton MR spectroscopy of human prostate at 3 T without Endorectal coil: feasibility. Radiology 245:507–516. doi:10.1148/radiol.2451061444

Song I, Kim CK, Park BK, Park W (2010) Assessment of response to radiotherapy for prostate cancer: value of diffusion-weighted MRI at 3 T. Am J Roentgenol 194:W477–W482. doi:10.2214/AJR.09.3557

Steyn JH, Smith FW (1984) Nuclear magnetic resonance (NMR) imaging of the prostate. Br J Urol 56:679–681

Sugahara T, Korogi Y, Kochi M et al (1999) Usefulness of diffusion-weighted MRI with echo-planar technique in the evaluation of cellularity in gliomas. J Magn Reson Imaging JMRI 9:53–60

Thompson IM, Pauler DK, Goodman PJ et al (2004) Prevalence of prostate cancer among men with a prostate-specific antigen level < or =4.0 ng per milliliter. N Engl J Med 350:2239–2246. doi:10.1056/NEJMoa031918

Turkbey B, Pinto PA, Mani H et al (2010) Prostate cancer: value of multiparametric MR imaging at 3 T for detection-histopathologic correlation. Radiology 255:89–99. doi:10.1148/radiol.09090475

Turkbey B, Shah VP, Pang Y et al (2011) Is apparent diffusion coefficient associated with clinical risk scores for prostate cancers that are visible on 3-T MR images? Radiology 258:488–495

Vicini FA, Vargas C, Abner A et al (2005) Limitations in the use of serum prostate specific antigen levels to monitor patients after treatment for prostate cancer. J Urol 173:1456–1462. doi:10.1097/01.ju.0000157323.55611.23

Wang L, Mazaheri Y, Zhang J et al (2008) Assessment of biologic aggressiveness of prostate cancer: correlation of MR signal intensity with Gleason grade after radical prostatectomy. Radiology 246:168–176. doi:10.1148/radiol.2461070057

Westphalen AC, Coakley FV, Roach M 3rd et al (2010) Locally recurrent prostate cancer after external beam radiation therapy: diagnostic performance of 1.5-T Endorectal MR imaging and MR spectroscopic imaging for detection. Radiology 256:485–492. doi:10.1148/radiol.10092314

Zakian KL, Sircar K, Hricak H et al (2005) Correlation of proton MR spectroscopic imaging with Gleason score based on step-section pathologic analysis after radical prostatectomy. Radiology 234:804–814. doi:10.1148/radiol.2343040363